VI International Conference on Computational Methods in Marine Engineering
MARINE 2015
F. Salvatore, R. Broglia and R. Muscari (Eds)

CAVITATION DYNAMICS AND UNDERWATER RADIATED NOISE SIGNATURE OF A SHIP WITH A CAVITATING PROPELLER

Da-Qing Li, Jan Hallander, Torbjörn Johansson and Roger Karlsson

SSPA SWEDEN AB

e-mail: da-qing.li@sspa.se, web page: http://www.sspa.se

Key words: propeller, cavitation, pressure pulses, underwater radiated noise

Abstract. The paper presents SSPA's work in the EU project AQUO to predict underwater radiated noise (URN) generated by a coastal tanker with a cavitating propeller. A CFD method, consisting of a multi-phase Delayed Detached Eddy Simulation (DDES) and a Ffowcs Williams-Hawkings (FWH) acoustic analogy, is applied to predict the cavitation, pressure pulses and radiated noise for the ship at model and full scale. In comparison with the data obtained from the model test and full scale measurement, it is found that the predicted sheet cavity correlates quite well with the observed ones in the experiment and sea trial. Some success is made in predicting the collapse and rebound of tip vortex cavitation (TVC) at model scale, yet the extension of TVC is under-predicted. The predicted pressure pulses agree reasonably well with the measured ones at the first three harmonics, deviation becomes larger at higher harmonics. The tonal noise has fairly good agreement with the measured signal at both scales up to 5^{th} harmonics. The simulation however under-predicts part of broadband noise that is caused by the TVC, mainly due to an under-resolution of the flow in the tip region and the propeller wake. The agreement with the data for the model scale case is slightly better than that for the full scale case.

1 INTRODUCTION

Propeller is recognized as a noise source that has dominant contribution to the underwater radiated noise (URN) in low frequency range among the noise sources of a propeller-driven ship. The occurrence of cavitation on propeller blades can further increase the noise level significantly. Excessive underwater noise pollutes the ocean environment and threatens marine life. It is no doubt important to understand the ship generated noise and its radiation characteristics. Equally important is computational tools to predict reliably the noise level generated by ships at and after design stage.

Methods for predicting noise generation and propagation can be classified into two broad categories. The first one is the direct computation of the generation and propagation of sound waves by solving time-accurate and compressible form of governing equations that are capable of resolving various turbulence length scales, such as Direct Numerical Simulation or Large Eddy Simulation (LES). The direct method is computationally expensive inasmuch as it requires highly accurate numerics, very fine meshes all the way to receiver locations, and acoustically non-reflecting boundary conditions. The computational cost becomes prohibitive when noise is to be predicted in the far field. The second category of methods decouples the sound propagation from its generation source, allowing one to separate the flow solution from the acoustic analysis. The flow solution is obtained by a less expensive method like URANS, DDES or a zonal LES, whereas the sound propagation is treated by an integral method based on acoustic analogy. Ffowcs-Williams and Hawkings (FWH) integration method[1] is such a method widely used in aerodynamics. A relatively new form of surface integration, called permeable (or porous) formulation is of particular interest. It allows for defining source surfaces not only on solid body surfaces but also on permeable (or porous) surfaces interior to fluid domain. The definition makes it possible to account for the contribution of the non-linear terms resulting from the instantaneous shear stress and vorticity content (quadrupole noise sources) in a highly turbulent flow domain enclosed by the permeable surfaces. The wake of the hull and propeller is such a domain. The application of the permeable formulation for non-cavitating propellers was explored by Testa et al.[9] and further investigated by Ianniello et al. [5][6][7] in which the important contribution of nonlinear quadrupole sources was shown and the inadequacy of RANS methods in solving turbulent fluctuations was addressed. The application for cavitating propellers was previously studied by Salvatore et al. [8] using a BEM method.

In our previous work[2], an URANS method coupled with FWH's acoustic analogy was applied to predict the noise generated by an LNG ship with a cavitating propeller. Although an overall qualitative agreement was achieved the study revealed an under-prediction of radiated noise by 25dB of the measured full scale data. It was realized that the inability to resolve turbulence length scales was the primary limitations of URANS methods. Consequently, the nonlinear noise source arising from the instantaneous stress tensor and the turbulent eddies in the hull-propeller wake are missing. In the present work a scale-resolving method of Delayed Detached Eddy Simulation (DDES), coupled with the permeable formulation of FWH's integration method is adopted to deal with the problem. It aims to assess how well a method of such can predict the cavitation dynamics and noise signature as compared with the measured data. The work is part of the on-going EU project AQUO (Achieve QUiter Oceans by shipping noise footprint reduction, www.aquo.eu).

2 MODEL TESTS AND SEA TRIAL

The subject ship is a 116.9 m long, 18 m wide coastal tanker equipped with a 4-blade left-hand CP propeller having a diameter 4.8 m, blade area-ratio 0.45 and design pitch ratio of 0.87.

A comprehensive experiment campaign was carried out in SSPA's towing tank and cavitation tunnel[3]. Cavitation observation, pressure pulse and noise measurement were performed at six loading conditions. **Figure 1** shows a photo of the ship model inside the

cavitation tunnel (left), a sketch of transducer locations for pressure pulse measurement (mid) and a sketch of the hydrophone locations for noise measurement (right).

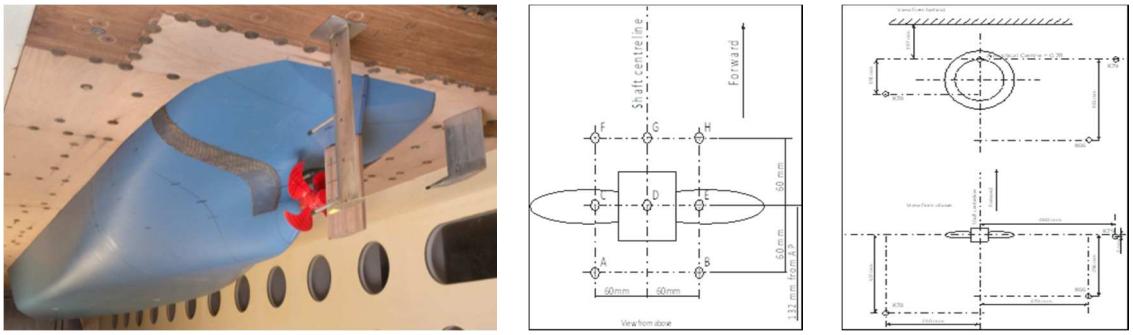

Figure 1: Model setup (left), sketch of transducer locations (mid) and hydrophone locations (right)

In addition to the model tests, SSPA conducted onboard vibration and pressure pulse measurement of the full scale ship, and onsite measurement of underwater radiated noise[4]. An underwater video camera was mounted outside the ship to record the cavitation behavior, the location of which is very close to transducer location F on the model hull.

The loading used in the simulations corresponds to loading condition LC2 defined in the report[3], i.e. at 15.4 kn service speed, NCR power with 15% sea margin and the propeller rotating at 120 rpm with design pitch. The estimated thrust coefficient is $K_T \approx 0.193$ and the cavitation number becomes $\sigma_n = 2.9$ at ballast draught.

3 NUMERICAL METHODS

DDES is a hybrid method that combines and switches between a RANS and an LES solver, depending on the local grid cell size and the relative distance to the wall boundary. Namely, RANS method is used to solve the flow inside the attached boundary layer and the LES is employed in the region of separated flow or wake wherever the grid is fine enough. For the turbulence modelling in the RANS part, SST k-ω turbulence model is used. Moreover, the subgrid scale turbulent viscosity in the LES region is also determined by the transport equation for k and ω. A special grid size based criterion is introduced into the dissipation term Y_k in the k-equation to activate the switch between the RANS and LES mode. The re-formulated dissipation term reads,

$$Y_K = \rho\beta^* k\omega S_{DDES} \tag{1}$$

The switch (or shielding) function S_{DDES} is expressed as:

$$S_{DDES} = \max\left(\frac{L_t}{C_{des}\Delta_{\max}}(1 - F_{DDES}),\ 1\right) \tag{2}$$

The C_{des} is a calibration constant (=0.61) used in the DES model and Δ_{max} is the maximum local grid cell spacing of (Δ_x, Δ_y, Δ_z). The L_t is the turbulent length scale defined in the RANS model. The function F_{DDES} is designed in such a way to give $F_{DDES} = 1$ inside the boundary layer

and ensures that LES mode will not be activated inside the boundary layer (hence avoiding or *delayed* the undesirable grid-induced separation), and $F_{DDES}=0$ away from the wall to regain the original form of DES shielding function. Cavitation is simulated by solving an additional transport equation for the vapor volume fraction with Zwart's cavitation model to account for the mass transfer between liquid and vapor phases. The formulation for FWH's acoustic analogy is described in detail in our previous work[2] and not repeated here. ANSYS Fluent v15.0 is used. The used numerical schemes are as follows:

- Multiphase mixture flow incompressible solver
- Pressure and velocity solved in a coupled manner
- Bounded 2nd order central difference for convection terms in momentum equations
- QUICK scheme in other transport equations
- Propeller rotation handled by sliding mesh technique
- Bounded 2nd order implicit scheme for time-derivative
- Time-step is $5.97\text{x}10^{-5}$ [s] at model scale and $6.94\text{x}10^{-4}$ [s] at full scale

The solution is accomplished in two steps. First, the flow field is solved with the DDES solver. During the precursor URANS simulation (before switching to DDES) K_T-identity method is used to adjust the blade loading by tuning the inflow speed while maintaining the rotational speed of propeller until the computed K_T approaches the estimated target K_T. In step two, the noise propagated from acoustic sources to an arbitrary receiver location is predicted by numerical integration of FWH's equation on the predefined source emission surfaces.

The sketch in **Figure 2** (left) shows the computational domain and boundaries. The inlet boundary is located at $1L_{pp}$ fore of FP and the outlet boundary $1.5L_{pp}$ aft of AP. The two sides and the bottom of the domain are placed $1L_{pp}$ away from the central line respectively. A smaller rectangular domain closely surrounding the hull is also visible in **Figure 2**. It has two roles: grid refinement is focused in this domain to facilitate an LES solution; the domain boundaries serve as the permeable integral surfaces later in the FWH acoustic analysis.

Constant velocity, turbulence intensity and viscosity ratio are specified at the velocity inlet boundary, whereas a constant pressure is set at outlet boundary to ensure correct cavitation number. The free surface, side and bottom boundaries are treated as slip walls.

All grids are of hexahedral type. The grids are refined not only in the wall normal direction to achieve a $y^+=1$, but also in the streamwise and girthwise direction to fulfil grid requirement for DDES method. For the full scale case, however, some compromises were made in the streamwise and girthwise direction to prevent the total number of grid cells from being prohibitively large. A grid cut-off at the central plane is shown in **Figure 2** (right). The black region that embraces the propeller is the sliding mesh rotating block. The total number of grid cells is about 35 million at model scale and 47 million at full scale.

4 RESULTS AND DISCUSSIONS

The results are presented in the following formats: Iso-surface of vapor volume fraction $\alpha_v=0.5$ is used to visualize cavitation surface. Turbulence vortex structure is represented by the

iso-surface of Q-criterion, defined as $Q=0.5(\Omega^2-S^2)$ [s^{-2}], in which S is the strain rate and Ω the vorticity rate magnitude. Pressure pulses in full scale case are given as amplitude in [kPa] and those in model scale case as K_p coefficient defined by $K_p = 2P_M/(\rho(nD)^2)$, where P_M being the single amplitude of pressure signal. No windowing scheme is applied to the noise signal. The noise is presented as sound pressure level of Power Spectra Density (L_{PSD}). The source level radiated noise (URN) is derived by scaling to 1 m distance away from the acoustic center.

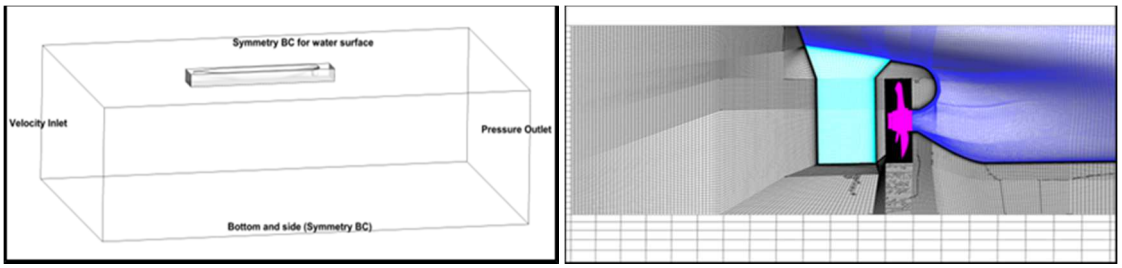

Figure 2: Computational domain (left) and grid cut-off at the central plane (right), model scale

4.1 Flow Field

The turbulent vortex structures in the wake of hull and propeller at model scale are shown in **Figure 3**(a) with an iso-value of Q=1000, and for the full scale in **Figure 3**(b) with a Q=200. As seen in the figure, the tip vortices and wake structures in the near downstream region are well captured. However, they disappear in a short distance downstream the rudder, indicating an insufficient resolution farther downstream. Compared with the full scale, more structures are captured at model scale especially for the tip vortices. The shielding function S_{DDES} in Eq. (1) is an indicator for LES resolved region when $S_{DDES} > 1$. The contour plots of S_{DDES} in the range $1< S_{DDES} < 10$ on the central plane are shown in **Figure 4**. The region of S_{DDES} below 1 and above 10 is cut-off in the plots, thus the hollows next to the dark blue area corresponds to the RANS region ($S_{DDES} \leq 1$) whereas the hollows next to the red area is well-resolved LES region ($S_{DDES} \geq 10$). The plots show that there are thin RANS regions very near the walls, meaning that the boundary layers are indeed solved by RANS as designed. The plots also reveal that there are undesirable RANS regions (hollows) downstream the rudder, beneath the propeller and the bottom of hull where the grid is too coarse to trigger an LES solution, since they occur inside the FWH integration domain where LES solution is desired. The undesirable RANS region appears to be larger for the full scale than the model scale case.

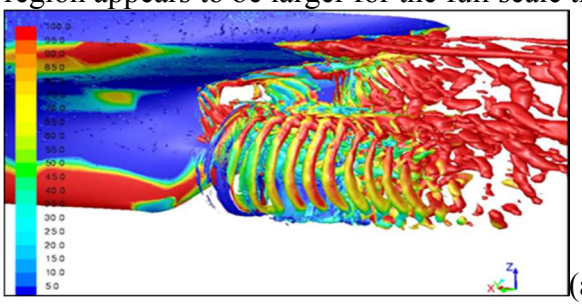
(a)
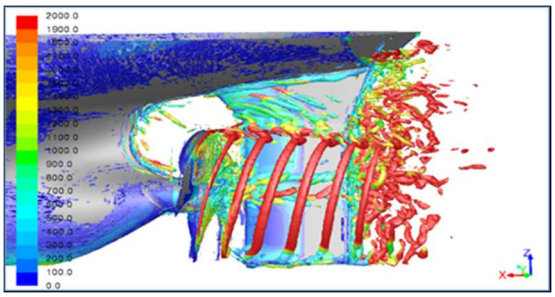
(b)

Figure 3: Turbulence vortex structures at model scale (a), and full scale (b)

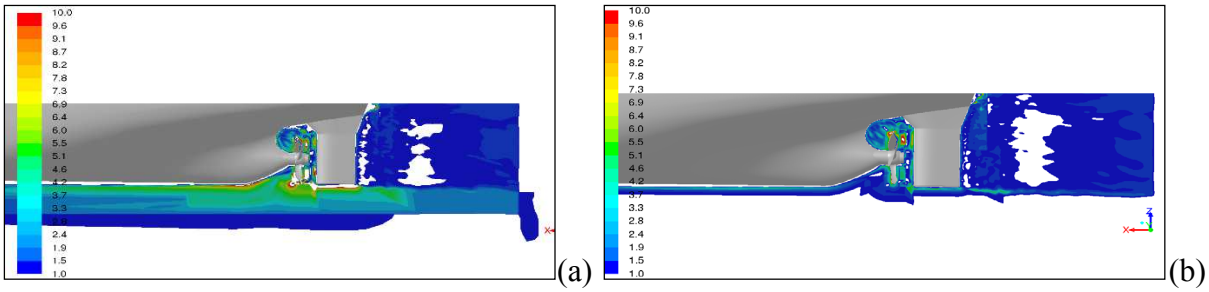

Figure 4: Contour plot of shielding function S_{DDES} on central plane at model scale (a), and full scale (b)

4.2 Model Scale

Cavitation behavior. The predicted cavitation is compared with that observed in the cavitation test at five blade angular positions in **Figure 5**. In the test, a narrow sheet cavity, a bit unstable, is observed on the suction side, starting from blade position θ=0° at radius r≈0.9R (with R being the propeller radius). The cavity varies its circumferential extension with angle θ and finally diminishes at θ≈60°. As the blade exits the wake peak, the cavity rolls up into a cavitating tip vortex visible up to θ≈70° (or at θ=340° in **Figure 5**). The predicted sheet cavity correlates quite well with that observed in the test, but the cavity starts earlier (at θ≈355°) at a lower radius r=0.8R. It extends slightly more in the chordwise direction and is rather stable. The characters for the sheet cavitation are shown at θ=10°, 30° and 50° in **Figure 5**.

The features representative for the tip vortex cavity (TVC) are visible at blade position θ=340° and 350° in **Figure 5**. In the experiment the TVC is a bit unstable and some bursting is observed. In the simulation, with a highly refined grid and a more rational turbulence scale resolving method, we note that some success is made in reproducing the TVC. The collapse and rebound of TVC is also seen in the animation (not shown). The downstream development of TVC is however obviously under-resolved compared with the model test, indicating an insufficient grid refinement in the local region.

Pressure fluctuations. The measured pressure pulses (PP) at the eight transducer locations are compared with the predicted ones in **Figure 6**. As seen there, the PP is highest at location D and second highest at G (see **Figure 1** for transducer location). The agreement with the measured PP at the 1st harmonic mode is quite good. The correlation at the 2nd and 3rd harmonics is reasonable. However, the computation over-predicts the PP at the 4th and 5th harmonics.

Noise signature. The predicted noise spectrum at receiver level is compared with the measured one in a frequency range up to 1.4 kHz in **Figure 7** for hydrophone K66 and K78 (see **Figure 1** for the hydrophone locations). The spectrum for hydrophone K79 is similar to these two and thus not shown here. The vertical grid lines in the diagrams are drawn at harmonics of Blade Passing Frequency (BPF) with a blade rate (BR) fundamental of 93 Hz for the model scale case. It is clearly seen for both hydrophones that the tonal noise at the first six BPF has good agreement with the data.

As to the broadband noise, the measured data reveals a distinctly high level in the frequency range around 700-1200 Hz. The noise spectra here are mainly attributed to the tip vortex cavitation and its bursting behavior. As seen in **Figure 5**, the DDES has somewhat under-

predicted the strength and downstream development of tip vortex cavity, which certainly will lead to an under-estimate of broadband noise. A secondary reason for the relatively large discrepancy in this frequency range could be the insufficient resolution of turbulence vortices farther downstream the rudder as shown in **Figure 4**. Note that the measured noise below the 1st BPF exhibits a higher level than the computed, since the measured noise contains also the background noise from the impeller operation in the cavitation tunnel and the impeller noise is predominant in the very low frequency range, some discrepancy between the computed and the measured noise below the 1st BPF is not surprising. **Figure 8** (left) compares the measured and computed URN at source level over the entire frequency domain, showing an overall reasonable correlation with the data.

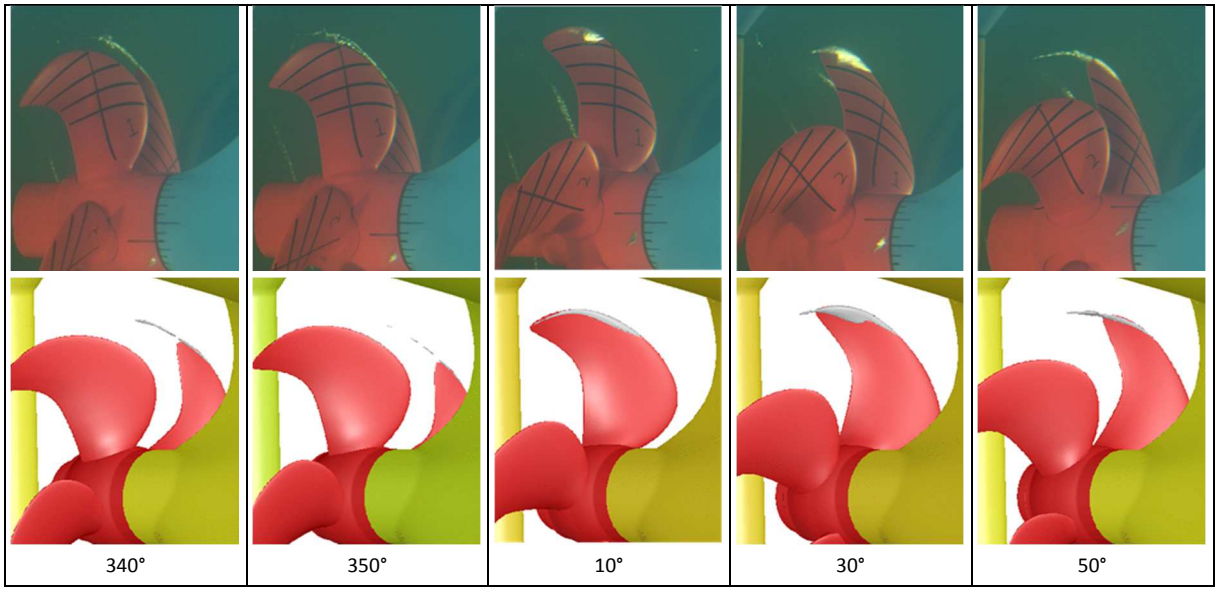

Figure 5: Cavitation pattern at model scale, Exp. vs. DDES

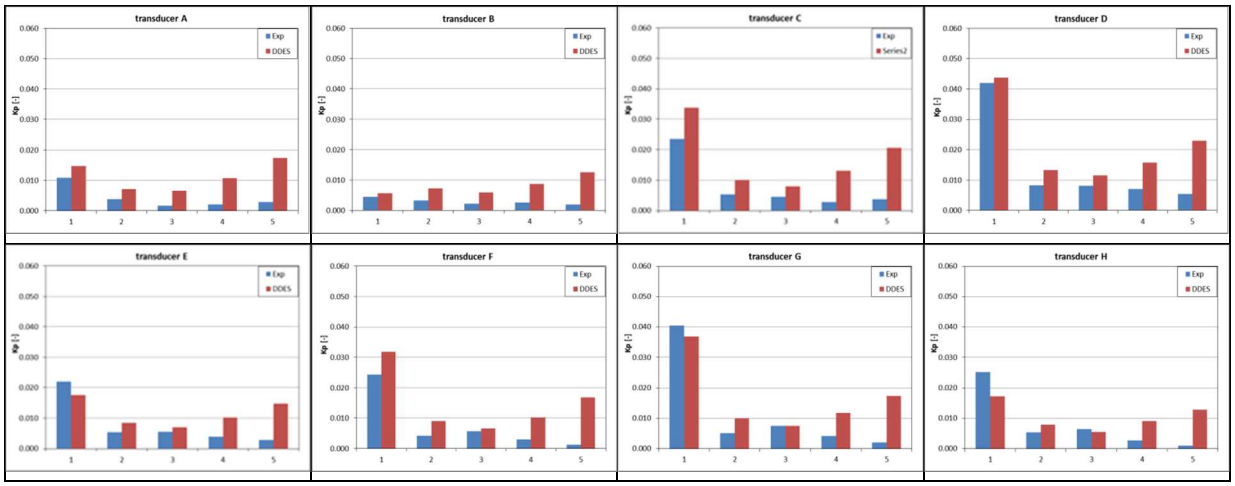

Figure 6: Pressure pulses at model scale, Exp. vs. DDES

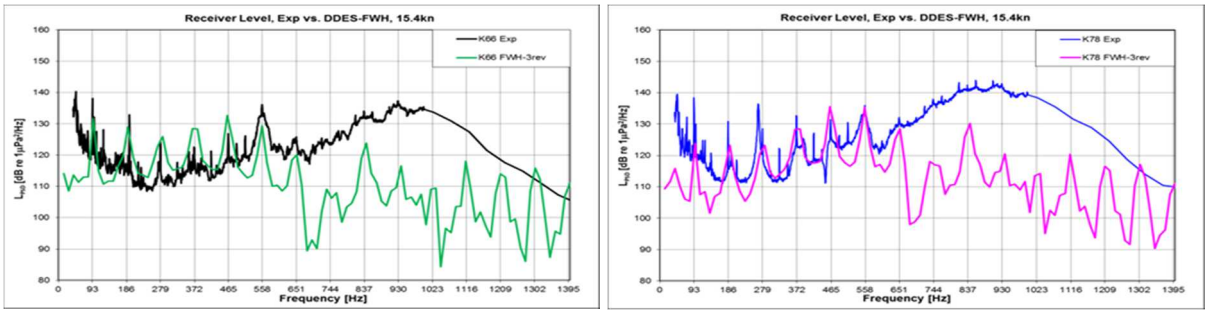

Figure 7: Receiver level noise at hydrophone K66 (a) and K78 (b), Exp. vs. DDES

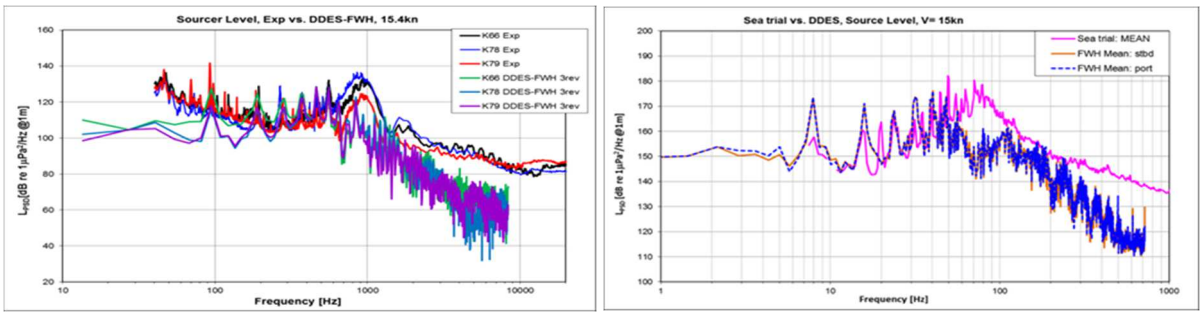

Figure 8: Source level URN, Exp. vs. CFD, model scale (left) and full scale (right)

4.3 Full Scale

Cavitation behavior. The full scale cavitation is compared with the video images from the sea trial in **Figure 9**. The simulation predicted a narrow sheet cavity on the suction side leading edge (marked by the blue ovals). As the blade exits the wake peak, it merges into a tip vortex cavity. The character is very similar to the cavitation behavior observed at model scale (**Figure 5**), except that the sheet cavity at model scale is slightly wider. As to the tip vortex cavitation, it is clearly seen (marked by red ovals in **Figure 9**) that the TVC observed in the sea trial persists longer distance downstream, whereas the predicted one is under-resolved and less developed downstream. Like in the model scale case, it is logical to expect that the part of broadband noise that is caused by the tip vortex cavity will become under-predicted in the simulation.

Pressure fluctuations. The full scale pressure pulses were measured at only one location, corresponding closely to the transducer location F at model scale. Therefore, the measured signal is compared with the predicted one at transducer F in **Figure 10**(a). The agreement at the 1st and 6th harmonic mode is very good. The amplitude for the 2nd to 5th harmonics is slightly higher than the measured ones. Starting from the 7th up to the 11th harmonics, the amplitude is however considerably under-predicted, the reason of which is discussed in connection with the under-prediction of broadband noise.

Noise signature. A rake of seven monitoring locations (numerical hydrophones) is defined on either side of the ship, in parallel with the center line. The locations relative to the acoustic center (AC) of the ship are illustrated in **Figure 10**(b). The AC is defined at a location on the center line 10 m distance forward of station 0. Since the full scale propeller is rotating at 120

rpm, the blade passing frequency (BPF) or the blade rate (BR) fundamental is 8 Hz and its harmonics read as 16, 24, 32, 40 Hz and so on. The noise spectra calculated at the hydrophone locations are averaged in different ways to reflect the possible directivity effect.

The source level PSD at the starboard and port side (after averaging the data at the 7 hydrophone locations along each side) are compared with the averaged full scale noise first in **Figure 8** (right). The figure gives an overview of the correlation between the computed and the measured noise in frequency range up to 1000 Hz in log scale. The same spectra in the low frequency range (up to 200 Hz) are then plotted in **Figure 11**(a). **Figure 12**(a) is the comparison for noise signature at 45° fore and 45° aft of the AC, and **Figure 12**(b) is for noise at 0° broadside. The vertical grid lines in these figures are drawn at the multiples of BPF.

Inspecting the measured noise spectra in **Figure 11**(a), one can see that there are a few spiky signals appearing in between the tonal noise at BR harmonics. They are caused by the prime engine and other auxiliary machineries. Their contribution to URN was analysed by Johansson et al. [4]. An example of the source identification diagram is given in **Figure 11**(b) to illustrate the complexity of measured data in the sea trial.

As seen in **Figure 11**(a), there is a fairly good agreement between the predicted and the measured tones at the 3rd to the 5th BPF, whereas the other tones are higher than the measured in the low frequency range and lower in the frequency range $f > 48$ Hz. In the frequency range $f < 16$ Hz, the processed noise from the full scale measurement is influenced by a likely underestimated transmission loss correction, therefore the processed sea trial data is likely lower than the reality and the computed one should be closer to the reality in this range. For broadband noise, a fairly good agreement is seen in the frequency range $f < 48$ Hz and $112 \text{ Hz} < f < 200$ Hz.

In the frequency range 48-112 Hz, there is however a significant under-prediction of broadband and tonal noise. The maximum under-prediction is about 28 dB at 72 Hz. Based on the source identification analysis of the full scale data in **Figure 11**(b), the high level noise in this range is mainly attributed to the persistent tip vortex cavitation observed in the sea trial. Recall that the DDES has under-resolved the TVC in the simulation, the under-prediction of noise in this range is thus an expected outcome. Similar under-prediction is also observed for the pressure pulses **Figure 10**(a) due to the same reason.

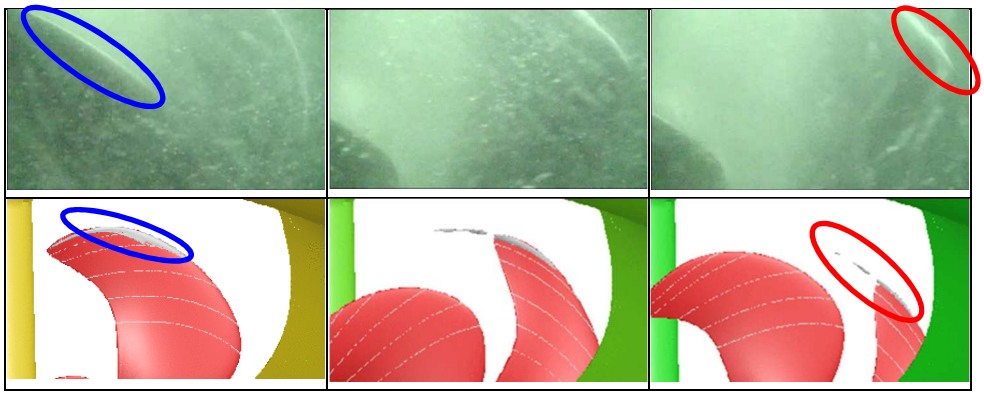

Figure 9: Cavitation pattern at full scale, video image vs. DDES

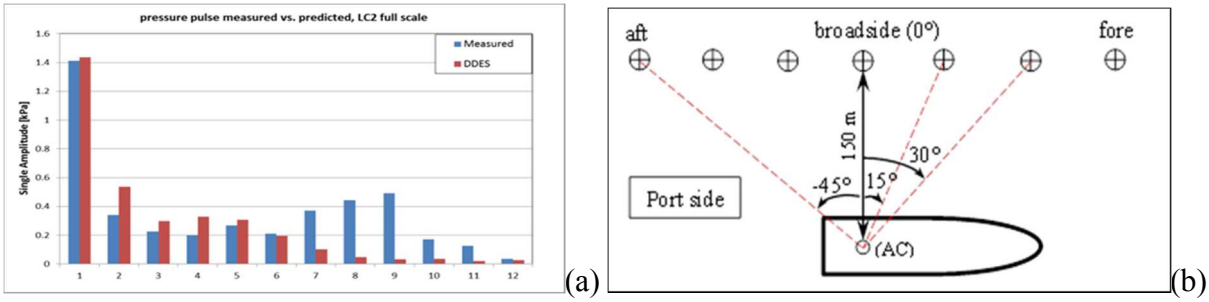

(a) (b)

Figure 10: Pressure pulses at full scale (a), and the full scale noise monitoring locations (b)

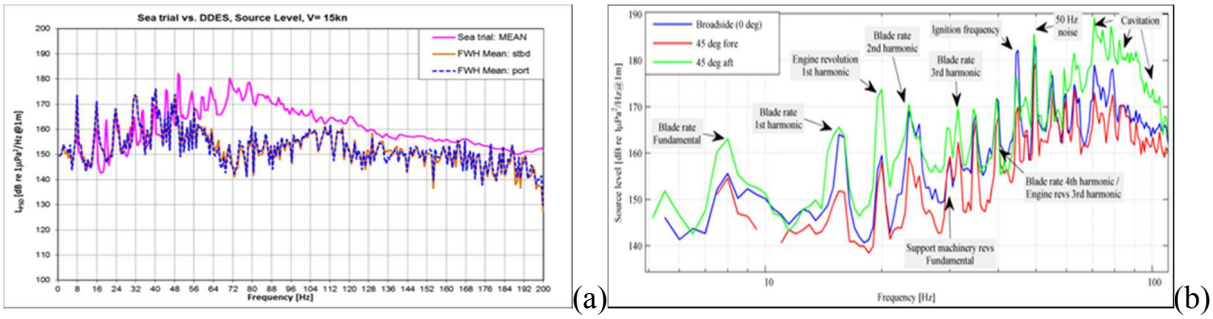

(a) (b)

Figure 11: The measured vs. predicted full scale URN low frequency range (a), and source identification (b)

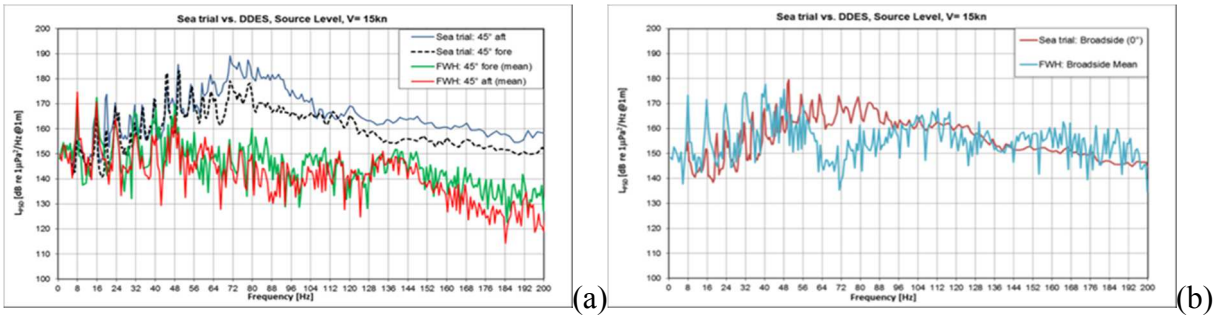

(a) (b)

Figure 12: Comparison of full scale averaged L_{PSD} at 45° fore and aft AC (a), and at 0° broadside (b)

The second observation in **Figure 11**(a) is the closeness of the port and starboard side spectra, showing almost no directivity effect between port and starboard side. On the other hand, there is some directivity effect in the streamwise direction, as can be seen from the deviation in the averaged spectra obtained from 45° fore and 45° aft of the AC in **Figure 12**(a), both for the sea trial and CFD data. The correlation between the sea trial data and the predicted noise is somewhat better for the receivers located in the same transverse plane as the AC, i.e. the receiver at 0° broadside, shown in **Figure 12**(b).

4.4 Prediction difference between RANS and DDES

The vortical structures in the wake of propelled hull obtained by RANS solution are compared with DDES solution in **Figure 13**. Despite that exactly the same mesh was used in

the two simulations, the amount of resolved turbulence vortices is fundamentally different. A RANS method models the effects of all length scales and gives only an integral length scale of the largest eddies, whereas DDES can resolve eddies whose sizes are greater than the minimum grid cell size. Therefore DDES is able to capture some part of turbulence vortices in the wake. Obviously this difference has a consequence on the predicted noise. The URN predicted by RANS-FWH and by DDES-FWH are shown in **Figure 14**(a) and (b). It is seen clearly that the noise level obtained by RANS-FWH is lower than the measured data and that by DDES-FWH. Moreover, the noise by RANS-FWH consists of mainly tones and seems to be lack of broadband content.

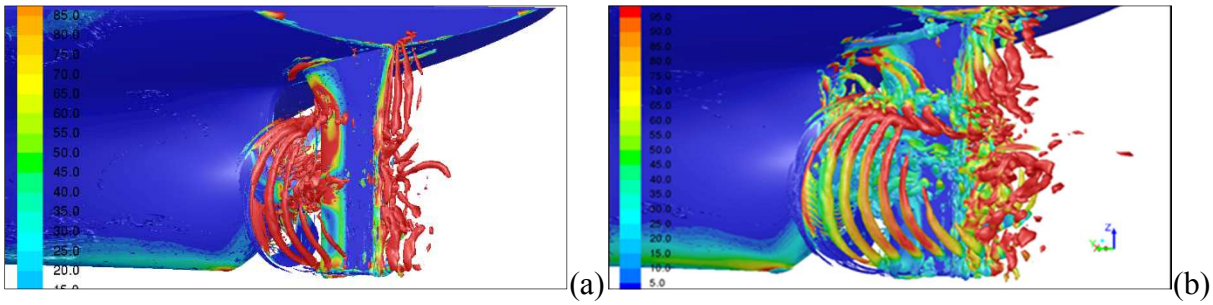

Figure 13: Turbulence structures visualized with Q=10000, URANS (a) vs. DDES (b) at model scale

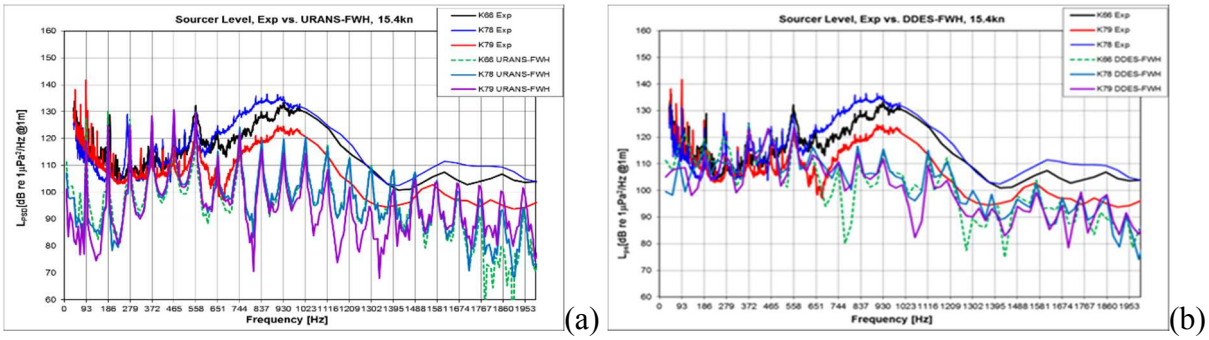

Figure 14: Source level noise predicted by URANS (a), and by DDES (b), model scale

5 CONCLUSIONS

A multiphase DDES method coupled with FWH's acoustic analogy is applied to predict the cavitation, pressure fluctuations and underwater radiated noise of a coastal tanker with a cavitating propeller in model and full scale respectively.

In comparison with the data obtained from the model test and full scale measurement, it is found that the predicted sheet cavity correlates quite well with the observed ones at both model and full scale. Some success is made in predicting the collapse and rebound of tip vortex cavitation (TVC) at model scale, yet the extension of TVC is under-predicted. The predicted pressure pulses agree reasonably well with the measured ones at the first three harmonics,

deviation becomes larger at higher harmonics. The tonal noise has fairly good agreement with the measured signal at both scales up to 5th harmonics. The simulation however under-predicts part of broadband noise at full scale in frequency range from 48 to 112 Hz that is caused by the tip vortex cavitation, mainly due to an under-resolved tip vortex cavity, which affects its contribution to radiated noise. The agreement with the data for the model scale case is slightly better than that for the full scale case.

Compared with URANS method used in a previous work, DDES is able to resolve some turbulent eddy structures and gives more account for the broadband noise. The DDES has however more stringent requirement on grid spacing, a further refined grid in the propeller wake would have resolved the tip vortices better and reduced the discrepancy from the measured data.

6 ACKNOWLEDGMENTS

This work was carried out within the collaborative project AQUO (Achieve QUieter Oceans by shipping noise footprint reduction), funded by the European Commission within the Call FP7 SST.2012.1.1-1: Assessment and mitigation of noise impacts of the maritime transport on the marine environment, Grant agreement No. 314227, coordinated topic "The Ocean of Tomorrow". The content of this paper does not reflect the official opinion of EU. Responsibility for the information and views expressed in the paper lies entirely with the authors.

7 REFERENCES

[1] Ffowcs Williams, J, E., Hawkings, D. L., "Sound generation by turbulence and surfaces in arbitrary motion", *Philosophical Transactions of the Royal Society*, A264, (1969).

[2] Hallander, J., Li, D-Q, Allenström, B., Valdenazzi, F. and Barras, C., "Predicting underwater radiated noise due to a cavitating propeller in a ship wake", *Proceedings of the 8th International Symposium on Cavitation (CAV2012)*, Singapore.

[3] "Propeller noise experiments in model scale". *AQUO Deliverable D2.4*, European Commission FP7 - Collaborative Project n° 314227, November 2014.

[4] Johansson, T., Hallander, J., Karlsson, R. Långström, A. and Turesson, M. (2015), "Full scale measurement of underwater radiated noise from a coastal tanker". *OCEANS' 15*, Genova, Italy.

[5] Ianniello, S., Muscari, R. and Di Mascio, A., "Ship underwater noise assessment by the acoustic analogy. Part I: nonlinear analysis of a marine propeller in a uniform flow", *J. Mar. Sci. Technol.* (2013), 18:547-570.

[6] Ianniello, S., Muscari, R. and Di Mascio, A., "Ship underwater noise assessment by the acoustic analogy. Part II: hydroacoustic analysis of a ship scaled model", *J. Mar. Sci. Technol.* (2014), 19:52-74.

[7] Ianniello, S., Muscari, R. and Di Mascio, A., "Ship underwater noise assessment by the acoustic analogy. Part III: measurements versus numerical predictions on a full-scale ship", *J. Mar. Sci. Technol*. (2014), 19:125-142.

[8] Salvatore, F., Testa, C., Ianniello, S., Pereira, F., "Theoretical Modelling of Unsteady Cavitation and Induced Noise", *Proceedings of the 6th International Symposium on Cavitation (CAV2006)*, The Netherlands.

[9] Testa, C. S. Ianniello, F. Salvatore and M. Gennaretti, "Numerical approaches for hydroacoustic analysis of marine propellers", *Journal of Ship Research*, (2008), Vol. 52, No. 1.